ACS Catalysis

Research Article

pubs.acs.org/acscatalysis

Exploring the Potential of Different-Sized Supported Subnanometer Pt Clusters as Catalysts for Wet Chemical Applications

Manuel Rondelli,[†,⊥] Gregor Zwaschka,[†,#] Maximilian Krause,[†] Marian D. Rötzer,[†] Mohamed N. Hedhili,[‡] Manuel P. Högerl,[§] Valerio D'Elia,[*,§,∥] Florian F. Schweinberger,[*,†] Jean-Marie Basset,[§] and Ueli Heiz[†]

[†]Technical University of Munich, Catalysis Research Center and Chemistry Department, Chair of Physical Chemistry, Ernst-Otto-Fischer-Straße 1 and Lichtenbergstraße 4, 85748 Garching, Germany

[‡]King Abdullah University of Science and Technology, Imaging and Characterization Core Lab, Thuwal 23955-6900, Kingdom of Saudi Arabia

[§]King Abdullah University of Science and Technology, Kaust Catalysis Center (KCC), Thuwal 23955-6900, Kingdom of Saudi Arabia

[∥]Vidyasirimedhi Institute of Science and Technology (VISTEC), School of Materials Science and Engineering, 21210, Payupnai, WangChan, Rayong, Thailand

Supporting Information

ABSTRACT: The use of physicochemical preparation techniques of metal clusters in the ultrahigh vacuum (UHV) allows for high control of cluster nuclearity and size distribution for fundamental studies in catalysis. Surprisingly, the potential of these systems as catalysts for organic chemistry transformations in solution has not been explored. To this end, single Pt atoms and Pt clusters with two narrow size distributions were prepared in the UHV and applied for the hydrogenation of *p*-chloronitrobenzene to *p*-chloroaniline in ethanol. Following the observation of very high catalytic turnovers (approaching the million molecules of *p*-nitroaniline formed per Pt cluster) and of size-dependent activity, this work addresses fundamental questions with respect to the suitability of these systems as heterogeneous catalysts for the conversion of solution-phase reagents. For this purpose, we employ scanning transmission electron microscopy (STEM) and X-ray photoelectron spectroscopy (XPS) characterization before and after reaction to assess the stability of the clusters on the support and the question of heterogeneity versus homogeneity in the catalytic process.

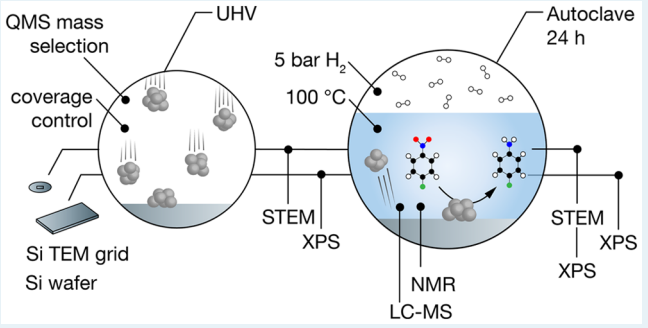

KEYWORDS: *subnanometer cluster catalysts, Pt atom catalysis, single atom catalysis, hydrogenation, size effects*

INTRODUCTION

Heterogeneous catalysis is of paramount importance for the chemical industry and contributes to the vast majority of its products, e.g., to the ammonia formation in the Haber-Bosch process[1] and the production of hydrocarbons from synthesis gas in Fischer−Tropsch synthesis,[2] to name just two.[3] Yet, a fundamental understanding of heterogeneous catalytic processes under applied conditions is very limited.[4] Besides successful attempts to elucidate the molecular processes on surfaces under well-defined reaction conditions in an ultrahigh vacuum,[5−8] another possibility to foster understanding is the preparation and use of single-site model heterogeneous catalysts where the structure of each active site is identical and well-understood.[9] These systems may allow deeper insights into the mechanistic aspects of the catalytic processes by the isolation of otherwise inaccessible active species, reaction intermediates, and byproducts and, in the long run, enable the preparation of more efficient catalysts with predictable activity and selectivity.[10]

One prime example for gaining access to such sophisticated systems is the surface organometallic chemistry (SOMC) approach[11−13] that has allowed unravelling of mechanistic details in reaction classes such as olefin[14] and alkane metathesis,[15,16] oxidative dehydrogenation of propane,[17] and CO_2 fixation to carbonates,[18] by supporting well-defined complexes and organometallic fragments of early transition metals on metal oxide surfaces.

Another approach is by means of surface science techniques and the use of complex and advanced physicochemical tools.[19−22] In this field, the use of cluster sources[23−26] and UHV techniques allows for coverage-independent preparation of supported cluster catalysts with either narrow, fine-tuned size-distributions or precisely tuned single-sized clusters, even down to one atom. Experimental studies with supported metal clusters in combination with theoretical calculations have

Received: February 16, 2017
Revised: May 8, 2017
Published: May 10, 2017

DOI: 10.1021/acscatal.7b00520
ACS Catal. 2017, 7, 4152−4162

proven to be powerful tools for the investigation of fundamental questions concerning catalysis, as they can be tailored atom by atom.[27−34] In general, the catalytic application of these systems has been, except for few examples,[35] limited to studies in the UHV regime, with pressures far from applied catalysis conditions. Nevertheless, in recent years, supported (size-selected) clusters were utilized under *ex situ* conditions for electrochemical[36,37] and photocatalytic[38,39] studies displaying remarkable size-dependent activity. Moreover, they have been applied as model systems for studies on sintering processes.[40,41] Despite these advances, to our knowledge, there is no application of UHV-prepared cluster catalysts as heterogeneous catalysts for organic reactions in solution.

To this end, samples with three different sized cluster ensembles were prepared using UHV techniques: either single atoms only (Pt_1) or unselected clusters with two different narrow size-distributions ($Pt_{n>1} \approx 2-20$ atoms or $Pt_{n>35} \approx 36-60$ atoms). After transfer to ambient conditions, we applied these materials as heterogeneous catalysts for the hydrogenation of solution-phase *p*-chloronitrobenzene as a test reaction.

The different and nonoverlapping cluster sizes were chosen to analyze the effect of Pt nuclearity on the catalytic performance. In particular, single atoms and the low-nuclearity clusters (often denoted in the literature as "pseudo-single" atoms) are of high interest as they represent the best conceivable form of noble metal dispersion and isolation on a support surface; they have recently been the subject of various mechanistic and catalytic studies.[42,43] The application of single atoms in catalysis has proved promising in granting both high activity at extremely low noble metal coverage and improved selectivity when compared to traditional systems.[44−49] Pt single atoms, in particular, have been applied for CO oxidation,[50−52] water gas shift reaction,[45,53] and the strictly intertwined process of hydrogen activation,[54] hydrogenation,[55] and hydrogenolysis.[56]

Our study addressed the following questions using a unique approach that combines the physical chemistry preparation and analytical characterization methods with applied catalysis testing in solution: Are such model systems suitable heterogeneous catalysts (a) for wet-chemistry conditions with regard to the performance and robustness of the clusters on the support or should they rather be considered as vectors of size-selected clusters for homogeneous catalysis (b) studies? Can there be size-dependent reactivity (c) in either of these circumstances?

RESULTS AND DISCUSSION

Catalyst Preparation and Experimental Approach. Scheme 1 depicts a summary of the study approach. Samples with three different sized cluster ensembles (Pt_1, $Pt_{n>1}$, and $Pt_{n>35}$) with independent control of size distribution and coverage were prepared using a laser ablation cluster source and a quadrupole mass spectrometer (QMS). The different ensembles were soft-landed under UHV conditions[23] onto two types of silicate support: Si wafers or Si TEM wafer grids. The latter where characterized using High-Angle Annular Dark-Field (HAADF)-STEM after transfer to ambient conditions. XPS (X-ray photoelectron spectroscopy) was employed to characterize the platinum clusters supported on Si wafers. These were subsequently tested for catalytic activity choosing the hydrogenation of *p*-chloronitrobenzene to afford *p*-chloroaniline (under 5 bar of H_2 pressure for 24 h at 100 °C in an autoclave) as a test reaction.

Scheme 1. Schematic Representation of the Experimental Approach Followed in This Study, Including Size-Selected Cluster Preparation, Catalytic Activity Testing, and the Analytical Techniques Employed for Cluster Characterization before and after Reaction

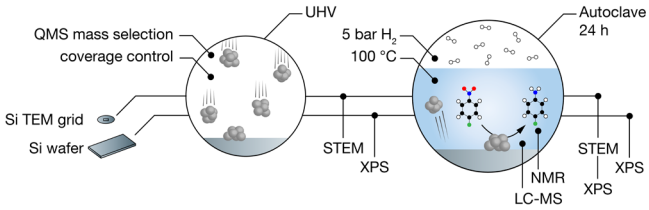

The product was quantified and identified by LC-MS analysis and its identity further confirmed by ^{1}H NMR spectroscopic analysis of the reaction mixture. To determine potential changes of the catalyst after the reaction, the used Si wafers were analyzed by XPS again. XPS and STEM were additionally performed on the clusters supported on the TEM grids after exposure to the same reaction conditions as the Si wafers to clarify potential support differences between TEM grids and wafers (consult Experimental Section section and SI for full experimental details).

Catalyst Characterization. For local catalyst characterization, HAADF-STEM was performed. Micrographs of two samples (Pt_1 and $Pt_{n>35}$) representative of different size regimes were recorded after transfer to ambient conditions and are displayed along with the corresponding analysis for the larger cluster ensemble in Figure 1.

The micrographs in Figure 1a and b show homogeneously distributed particles over the support for the single atoms and for the larger clusters. For each sample, the clusters are monodispersed and resemble each other, whereas the two samples differ by the particles' size.

For the Pt atoms, representative line scans (displayed later in the section dedicated to the catalyst stability) show isolated platinum atoms on the support after transfer to ambient conditions. The size (width of the line profile peaks) fits the expected size of the atoms. Observations of Au atoms by means of HAADF-STEM on an oxide support have been reported in the literature, and the obtained results for Pt resemble the results of the Au catalyst with respect to size and appearance.[57]

Particle detection based statistics for multiple images of unselected $Pt_{n>35}$ clusters (>400 analyzed particles) were performed. The area distribution function (ADF) of the larger clusters (Figure 1c) follows a log-normal shaped size distribution reflecting the production of the cluster source (see representative mass scan shown in Figure 1d and the SI), transmissions of the ion optics, and the quadrupole mass spectrometer used in the high pass filter mode as previously reported.[37,38,40]

Besides local characterization of the samples (Pt_1 and $Pt_{n>35}$), XPS measurements were performed as an integral characterization technique for all sizes/ranges on the wafer support, and the obtained spectra are shown in Figure 2.

For all samples, the survey spectra (Figure 2a) show signals of Si and O from the underlying support and C, a ubiquitous impurity, at the expected binding energies. Further, the characteristic Pt 4d and Pt 4f double peaks of the Pt cluster catalyst can also be clearly identified in the spectra, except for

DOI: 10.1021/acscatal.7b00520
ACS Catal. 2017, 7, 4152−4162

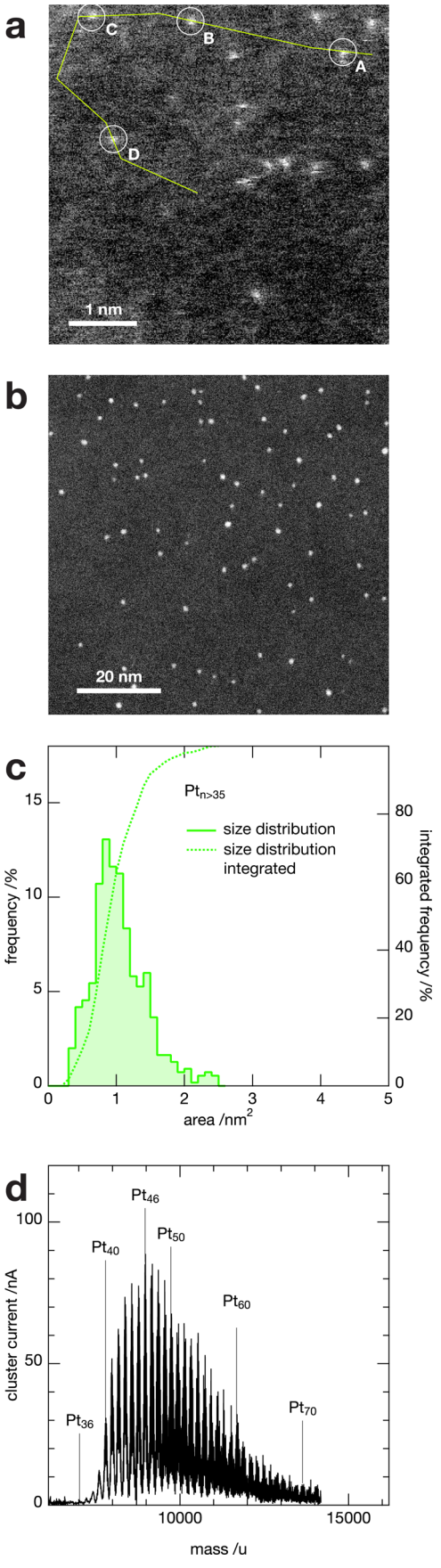

Figure 1. Representative HAADF-STEM micrographs of soft-landed Pt_1 (a) and $Pt_{n>35}$ (b) cluster catalysts on Si TEM grids; corresponding area distribution function (ADF; ensemble of >400 particles) for $Pt_{n>35}$ (c) and mass scan for $Pt_{n>35}$ (d) as selected by the QMS showing the size distributions of Pt_n^+ clusters optimized on mass Pt_{46}.

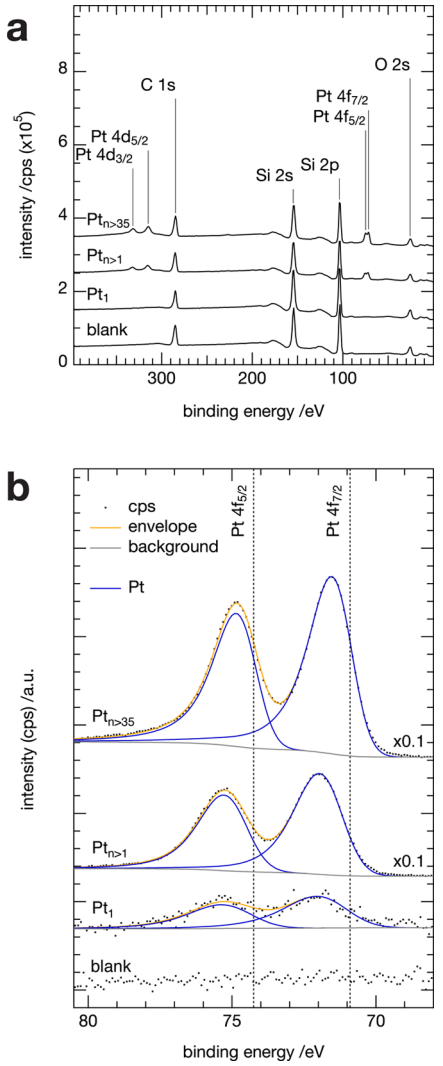

Figure 2. XP spectra of the pristine wafer supported Pt_1, $Pt_{n>1}$, and $Pt_{n>35}$ samples and the blank support: survey scans (a) and excerpts of the Pt 4f region along with the bulk Pt 4f literature values represented as dotted lines (b). The excerpts of the Pt 4f region reveal clear proof for the Pt presence in contrast to the baseline of the blank sample. For better visibility, the intensity signals of the data are plotted in arbitrary units (a.u.).

the blank, which is further proof for successful catalyst preparation.

The Pt 4f signal was chosen for a further assessment of the prepared samples, and it is shown in larger detail (Figure 2b). The different pristine samples show, as previously reported,[33,58] an increasing shift to higher binding energies for the Pt 4f peak with decreasing particle size when compared to the Pt bulk values as a reference (70.9 eV for $4f_{7/2}$, and spin orbit splitting of 3.3 eV).[59] The measured shift in the range of less than 1 eV for all samples (compared to up to 3 eV for the stoichiometric compound) is well-known and to a large extent attributable to an electrostatic final state effect for clusters[59,60] and, to a minor

DOI: 10.1021/acscatal.7b00520
ACS Catal. 2017, 7, 4152−4162

part, to the support (see argumentation in the section Support Effects).

On the basis of the results of STEM and XPS, a successful preparation of the different cluster catalyst materials is confirmed. Before drawing a conclusion on the stability of the catalyst material, we turn toward the second major question of this study, the chemical reactivity of the catalysts with respect to different sizes/size ranges.

Catalytic Experiments. The hydrogenation of *p*-chloronitrobenzene was employed as a model reaction in order to assess the catalytic activity of the clusters. After 24 h of reaction (see Experimental Section section for details), the product identity and yield were determined by LC-MS measurements. The formation of the desired product was additionally confirmed by ^{1}H NMR analysis of the crude reaction mixture (see Figures S5–S7) showing the exclusive formation of the target *p*-chloroaniline product.

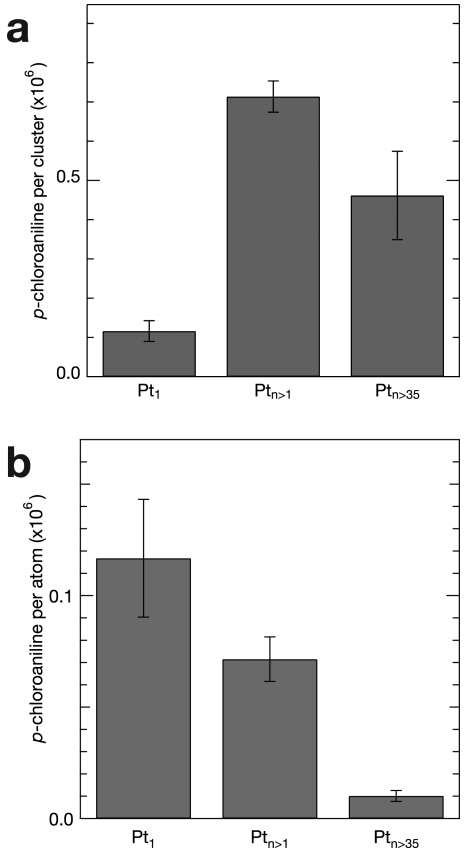

Figure 3. Catalytic activity expressed as yield of *p*-chloroaniline, as determined by LC-MS measurements after 24 h of reaction: per cluster size (a) and per atom in the cluster (b). Each bar-graph value is based on measurements of multiple samples, and the errors are derived from the resulting standard deviation of each sample.

The results of the catalytic tests are depicted in Figure 3. The results are corrected for the activity of a blank chip measurement and normalized with respect to the individual number of clusters ($Pt_{n>1}$ and $Pt_{n>35}$) and atoms (Pt_1) for each sample, based on the measured coverage (Figure 3a). All three cluster sizes showed activity toward the hydrogenation reaction and full selectivity toward *p*-chloroaniline. Significantly, different catalytic activity was found for the three cluster sizes/size ranges Pt_1, $Pt_{n>1}$, and $Pt_{n>35}$ (see SI for absolute values). The catalysis results were normalized in terms of activity per atom (Figure 3b) using the most abundant size for the unselected clusters (10 atoms for $Pt_{n>1}$ and 46 atoms for $Pt_{n>35}$, see SI for details) showing an important change in the activity trend. The single Pt atoms are now the most catalytically active, outnumbering the larger $Pt_{n>35}$ clusters by a factor of 17 and the $Pt_{n>1}$ cluster by over a factor of 2, per atom. For the larger sample $Pt_{n>35}$, not all atoms are exposed to the surface; i.e., a dispersion of about 60–70% has to be considered.[58] Thus, the observed activity per exposed atom is slightly less than twice the value shown in Figure 3b, however, still well below that of single atoms and $Pt_{n>1}$ clusters. Moreover, this has no influence when calculating the activity per mass Pt.

Pt single atoms and subnanometer clusters have been recently used, for the hydrogenation of nitroarenes displaying, in general, higher activity and selectivity toward the hydrogenation of nitro groups than that of larger Pt clusters on classical supports such as C and SiO_2.[61−64] In particular, single and pseudosingle atoms of platinum (cluster size <0.8 nm) supported on FeO_x were able to catalyze the selective hydrogenation of 3-nitrostyrene to 3-vinylaniline at 40 °C under 3 bar of H_2 with a turn over frequency (TOF) of about 1500 h^{-1}.[61] Zhang et al. have reported single Pt atoms supported on phosphomolybdic acid on activated carbon able to selectively convert nitrobenzene to aniline at room temperature under 10 bar of H_2 (TOF = 774 h^{-1}).[62]

A comparison of the catalytic performance of our catalysts and the reported heterogeneous catalytic systems employing single or pseudosingle Pt atoms for the hydrogenation of the nitro group of nitroarenes is reported in Table S6 in terms of turnover numbers (TON); additionally, the TOF values for our Pt clusters are available in the SI (Table S4). In spite of the variety of reaction conditions and substrates reported in the different studies, it is possible to see that considerably high TONs were obtained with Pt_1 and $Pt_{n>1}$, thus confirming the potential of isolated atoms and subnanometer clusters in affording highly active catalytic systems in the presence of very low noble metal loadings.

The higher activity of the single atoms can be rationalized by considering various factors: first, the increased degree of noble metal dispersion compared to larger clusters/particles with all the metal atoms, being, in principle, available for catalysis. This is in good agreement with the observation that the hydrogenation of nitro compounds by clusters of noble metals generally depends on the cluster size, and it is found to proceed more efficiently with smaller nanoparticles.[65,66] Importantly, the work of Sykes et al. has shown the remarkable capability of palladium and platinum single atoms to induce both facile H_2 activation and low-barrier desorption from the noble metal atom when compared to larger clusters.[44,54] These factors can have a strong impact in enhancing the catalytic performance of single atoms. It should also be noted that the electronic properties of the differently sized Pt clusters in this study vary as observed on the basis on the progressive shift toward higher binding energies of the Pt 4f binding energies in the XP spectra of Figure 2b. This behavior highlights an additional difference between the single atoms and larger clusters that could have an effect on the capability to interact with H_2.[67]

Interestingly, the activity of single Pt atoms observed by us and other authors[61−64] in the reduction of nitroarenes is at variance with other catalytic applications for which single atoms have not been found active.[68,69] In the oxidation of thiophenol with O_2 by gold single atoms, Corma et al. have demonstrated

DOI: 10.1021/acscatal.7b00520
ACS Catal. 2017, 7, 4152−4162

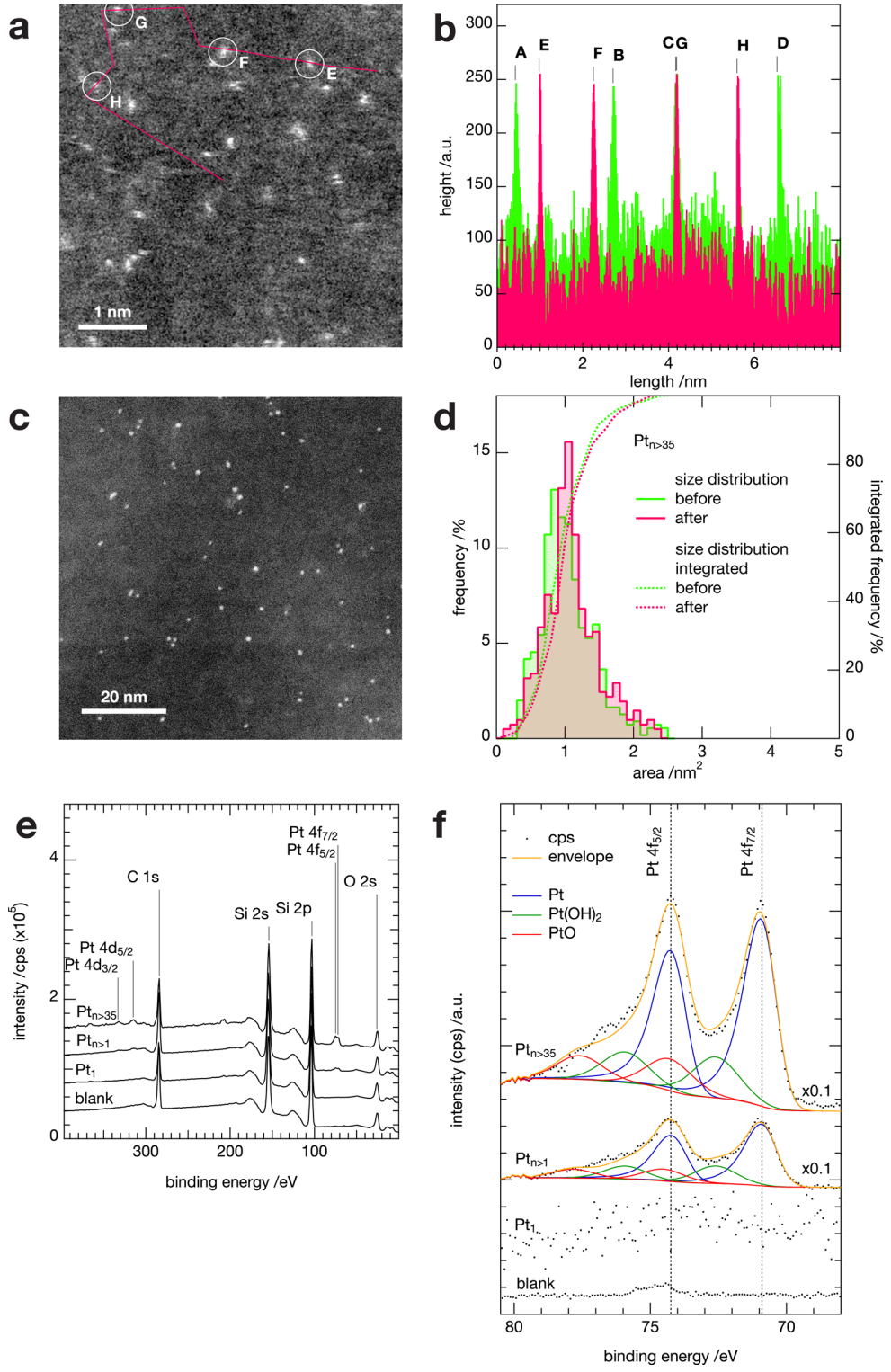

Figure 4. STEM micrographs of the Pt_1 (a) and $Pt_{n>35}$ (c) clusters on TEM grids after exposure to the reaction conditions. Analysis of the atoms/clusters before and after exposure to reaction conditions: line profiles for Pt_1 (b) and ADF for $Pt_{n>35}$ (d). XP spectra of the wafer supported samples Pt_1, $Pt_{n>1}$, and $Pt_{n>35}$ and of the blank support after the catalytic reaction: survey scans (e) and excerpts of the Pt 4f region (f). The expected XPS binding energy (BE) for bulk Pt 4f is represented as dotted lines. For better visibility, the intensity signals of the data are plotted in arbitrary units (a.u.).

the inability of single atoms to coordinate and/or activate both the substrate and O_2.[68] A possible role of the support in assisting the activation of hydrogen in nitroarenes hydrogenations has been proposed for Au clusters supported on Al_2O_3[65] and for Pt single atoms on FeOx,[61] but this seems unlikely to occur on a nonreducible support such a silica. Considering that nitroarenes adsorb well on silica materials,[70] the support surface could provide, in our case, the substrate for hydrogenation by the single Pt atoms. This, might take place through a series of successive hydrogenation steps producing

DOI: 10.1021/acscatal.7b00520
ACS Catal. 2017, 7, 4152−4162

nitroso and hydroxyamino intermediates.[71,72] However, it should be noted that Zhang et al.[62] have proposed that both hydrogen and substrate activation occur on a single Pt atom for their Pt_1/phosphomolybdic acid system without participation of the support. They have also calculated that coadsorption of H_2 and of the hydrogenation substrate results in a much higher adsorption energy than the adsorption of the substrate alone. It is clear that the main mechanistic aspects of nitroarene hydrogenation by single atoms are yet to be fully clarified, and they are likely to be strongly support-dependent.

Catalyst Stability. Additional experiments using the different samples were carried out in order to assess a potential loss of Pt atoms and clusters into the solution and the resulting impact on the catalytic activity. In the case of the single and pseudosingle atom clusters that have been recently applied for the successful hydrogenation of nitroarenes,[61−64] there is, in general, a lack of detailed studies on the occurrence of Pt loss and on its contribution to the observed catalysis results. Similarly, the postreaction characterization of the clusters is missing in most cases (one rare exception: single Pt atoms on FeO_x).[61]

First, we studied the reusability of the recovered catalysts for a second experiment under the same reaction conditions. Lower or no measurable reactivity was found (results not shown) during the second experiment for exemplary individual samples compared to the first run. This observation is a result of either the detachment of the clusters into the solution during the first run or a process of deactivation/oxidation of the clusters, as assessed by the appearance of new Pt species (predominantly oxides) in the XP spectrum of the catalysts after reaction (*vide infra*).

Second, in order to gain insight into the impact and occurrence of homogeneous catalysis, we carried out an additional set of experiments akin to a "hot filtration test," representatively with Pt_1 samples as the most catalytically active. This approach is generally applied in heterogeneous catalysis to assess the influence of homogeneous species on catalytic performance (by removal of the heterogeneous catalyst during the reaction and allowing it to proceed only in the presence of homogeneous species).[73,74] In experiment I, a previously unused Pt_1 catalyst was exposed to standard reaction conditions, but without the addition of *p*-chloronitrobenzene. After 24 h under these conditions, the catalyst was removed from the reaction vessel and transferred into a second vessel (experiment II). The substrate was added to both experiments, and the reactions were started by adding 5 bar of H_2 at 100 °C for 24 h. Experiment I showed a reactivity that was a factor of 200 higher than experiment II and was comparable to the performance of the original Pt_1 results (see SI for data). This clearly shows that the major part of the observed catalytic activity is provided by Pt atoms that are transferred into the solution and might act as homogeneous catalysts. The loss of these atoms makes the sample nonreusable in further catalytic runs and explains the lack of activity of the recycled sample and of experiment II. Additionally, the higher activity of about a factor of 3 in favor of experiment I, when compared to the experiment employing the pristine Pt_1 catalyst (see Tables S3 and S4), can be explained by considering that, in the former case, the substrate is added after 24 h with the wafer under the reaction conditions and could contain a higher initial concentration of homogeneous platinum.

In order to further assess the stability of the catalysts, STEM (for the clusters on the TEM grid) and XPS (for the clusters on the Si wafers) measurements were performed after the reaction or, for the cluster on the TEM grids, after exposure to the same reaction conditions as the Si wafers. In both cases, the analysis was compared with the STEM and XPS results of the corresponding fresh samples. Figure 4 displays a summary of these results: STEM micrographs after exposure to the reaction conditions (a,c), corresponding (statistical) analysis (b,d) with comparison to the data from before the reaction (see Figure 1), and an overview XP spectrum (e) as well as an excerpt from the 4f region (f).

From the TEM results, homogeneously distributed, monodisperse atoms or larger clusters after exposure to the reaction conditions are visible (Figure 4a,c), resembling those from before the reaction (Figure 1). Clearly both sample types (Figure 4a vs c) are still different with respect to the size for the different samples and homogeneous in size for each individual sample.

Representative line scans of the Pt_1 sample before (Figures 1a and 4b: A−D) and after (Figure 4a,b: E−H) confirm the presence of isolated platinum atoms on the support prior and after exposure to the reaction conditions. For both selected Pt_1 samples, sharp peaks corresponding to monodisperse ensembles with only atoms are visible. The size (width of the line profile peaks) fits the expected size of the atoms, and the atoms remain unaltered after exposure to the reaction conditions, suggesting that no agglomeration of atoms on the TEM-grid support has occurred. Repeating the statistical analysis of the $Pt_{n>35}$ sample after exposure to reaction conditions (Figure 4d), it was found that based on the ADF and the integration of the function, the cluster size of the larger clusters on the STEM grid support is not altered either (Figure 1c).

The overall interpretation of the results of this local analysis leads to the preliminary conclusion that neither ripening nor agglomeration can be observed for the atoms and clusters on the TEM grids.

Besides local characterization, XPS measurements were also performed for all sizes/ranges on the wafer support after the reaction, and the obtained spectra are shown in Figure 4e,f. After reaction, Pt can still be detected in the XP spectra (Figure 4f); however, a number of changes occurred. First, the intensity of the Pt 4f peaks decreased; in the case of Pt_1, no fitting of the measured signal was attempted due to its very low intensity. Consistently, an increase in the Si/Pt peak area ratio (see Table S2 in the SI) was observed for all samples, suggesting a loss of Pt. In proportion, the loss of Pt appears stronger in the case of $Pt_{n>1}$ with a reduction of the Si/Pt ratio of a factor of 6, and it is lower when considering $Pt_{n>35}$ (factor of 3) and Pt_1 (factor of 2). The inferred loss of Pt could arise from the detachment of Pt clusters or atoms from the support into the solution during reaction as a consequence of the relatively weak interaction between the noble metal particles and the unfunctionalized silica surface.[75,76] Second, the position of the main Pt peak shifted toward the binding energy of bulk Pt, likely as an effect of an increase in the size of the particles (which is in contrast to the TEM results). Moreover, the Pt 4f peaks became broader and more asymmetric after reaction, suggesting the buildup of oxidized platinum species with a shift >1 eV from the main Pt peak. Therefore, fits corresponding to $Pt(OH)_2$ and PtO were added to the fitting of the Pt 4f region: $4f_{7/2}$ peaks at 72.7 and 74.4 eV (with fixed spin orbit splitting of 3.3 eV), respectively, that are in a good agreement with the literature values.[77] This partial change in the oxidation state of Pt upon reaction can be

DOI: 10.1021/acscatal.7b00520
ACS Catal. 2017, 7, 4152−4162

attributed to the treatment with ethanol at 100 °C in the presence of some atmospheric oxygen in the reaction autoclave.

These results confirm the low stability of the clusters on the Si wafers. According to these observations, the catalytic data shown in Figure 3 need to be revised by assuming that the observed activity arises, to the largest part, from the portion of clusters that detached into the solution and act as homogeneous phase catalysts. On the basis of these corrected values (Table S6, entries 9−11), Pt_1 and $Pt_{n>1}$ still display size-dependent catalytic activity, and in both cases, these are still about 1 order of magnitude higher than that shown by the larger clusters of $Pt_{n>35}$. A comparison with the performance of other catalytic systems employing Pt nanoparticles (stabilized by ionic liquids[78,79] or N-heterocyclic carbenes[80]) in solution for the hydrogenation of chloronitroarenes (Table S6, entries 9−13) highlights the remarkable catalytic performance of the clusters prepared in this study as low-loading hydrogenation catalysts.

Interestingly, metal clusters in the solution phase have, to our knowledge, so far only been produced by the Brust−Schiffrin reaction[81] or by the polyol method[82] in which the clusters are capped by strongly bound reagents or by more loosely coordinated hydroxyl functionalities, respectively. Alternatively, cluster ensembles have been obtained by laser ablation methods in solution,[83,84] or by electrochemical methods.[85] Nevertheless, ultimate control of atomic precision in solution is generally limited to a small number of so-called "magic number" clusters.[86−88] A recent development in this field has been reported by Yamamoto et al. with the preparation of Pt clusters within dendrimers with nuclearity in the 12−20 range.[89] However, so far, no method for the size selection in solution for a wide range of cluster sizes as well as single-sized clusters has been achieved for Pt.

Support Effects. It is well-known that metal clusters, single atoms, and larger nanoparticles of noble metals applied for catalysis tend to leach and aggregate.[46] This is particularly true for nonreducible supports such as silica, and it is a consequence of the weak interaction between the noble metal and the silica surface.[90] In order to understand the difference in stability between the clusters deposited on Si wafers (as observed on the basis of XPS analysis and catalysis results) and the corresponding clusters deposited on the TEM grid (as observed on the basis of STEM analysis), we performed additional XPS measurements on a Si TEM grid of a $Pt_{n>35}$ sample after exposure to the reaction conditions. We focused on two aspects: a potential difference between the silicon oxide support of the TEM grids and the wafer as well as the influence of the support on the clusters. The excerpts of the relevant Si 2p and the Pt 4f region are shown in Figure 5 along with fits, comparing the two supports and the supported particles.[91]

Both supports show broad asymmetric peaks that arise from the presence of oxidized Pt species. Fitting of platinum-oxide species and the assignment of oxidation states for the studied systems is not a simple task.[92] Yet, we performed tentative fits also for the TEM grid support to elucidate the present form of oxides and could extract reasonable results under the assumption that elemental Cu ($3p_{3/2}$; reported at 75.1 ± 0.2 eV)[93] is also present in the Pt 4f peak area as an impurity from the treatment of the TEM grid in the microscope (i.e., grid holder). With respect to the Pt 4f region, one can see that the binding energy values of the Pt 4f peaks for the clusters on the TEM grid that were exposed to the reaction conditions are still shifted toward higher values as expected for the as-deposited

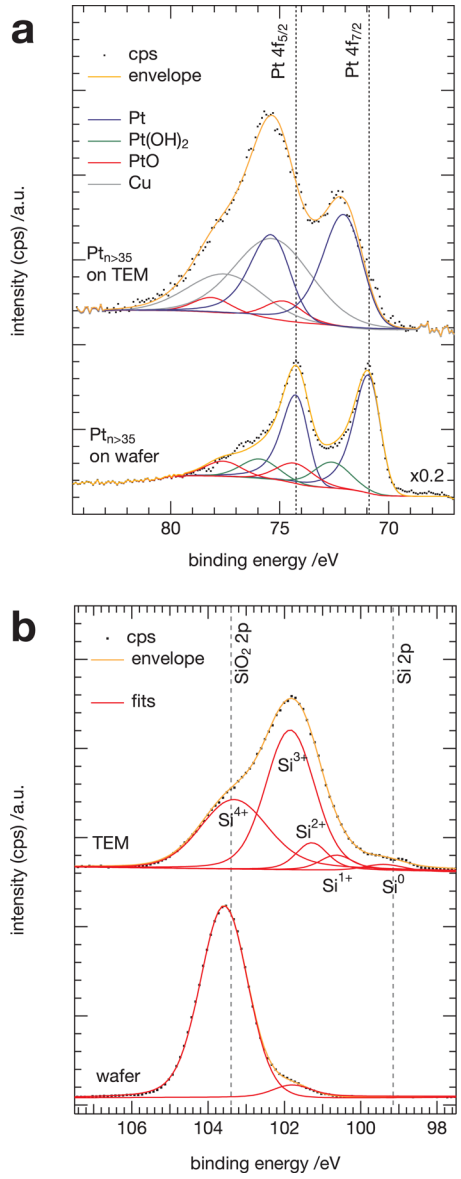

Figure 5. (a) Pt 4f peak region of the XP spectrum of $Pt_{n>35}$ on Si wafer (bottom) and on TEM grid (top) measured after exposure to the reaction conditions. (b) Si 2p peak region of the Si wafer and of the TEM grid. For the TEM grid, various Si oxidation states are assigned and visualized by the shown fits. The dashed lines show the literature BE for elemental Si(0) 2p (99.2 eV) and for SiO_2 (103.4 eV).

clusters (see Figure 2). This suggests that, in contrast to the wafer supported clusters, they do not seem to have sintered or agglomerated to bulk Pt upon treatment.

A drastic difference in the SiO_2 support material can be observed when studying the Si 2p region. For the wafer (with an artificially thermally grown SiO_2 layer), a slightly asymmetric SiO_2 peak (originating from the unresolved 3/2 and 1/2 2p spin−orbit coupling) at around 103.5 eV is visible and close to the literature value for stoichiometric SiO_2.[94] No indication for pristine Si (the Si(0) 2p shift is expected at 99.2 eV,[94] see dotted line in Figure 5b) and only minor Si species with oxidation states +I to +III are visible as indicated by a shoulder at around 101.5 eV. In contrast, the TEM grid, which is etched out of a Si wafer material, has a completely different surface composition with respect to the oxidation states that can be

DOI: 10.1021/acscatal.7b00520
ACS Catal. 2017, 7, 4152−4162

found. Here, the stoichiometric SiO_2 is not the most abundant species, but a broad signal with a maximum at around 102 eV and a broad tail toward the higher binding energy region is found. Therefore, the surface of the TEM grid has a very heterogeneous composition with different oxidation states of Si (ranging from SiO_2 to metallic Si) that could be assigned.

Combining the results from the analysis of the silicate materials, it can be inferred that the difference in the underlying supports has an influence on the stability of the clusters: the higher stability of the clusters on the TEM grid might be explained by the availability of less oxidized silicon that results in a stronger particle support interaction, since metals (Pt) tend to adhere to other metals (Si) very strongly.[95] Further, since the clusters on the grid display a higher degree of oxidation, upon exposure to the reaction conditions, than on the wafer support, this partial oxidation of the clusters might help in decreasing the tendency toward detachment and aggregation.[96]

On the other hand the influence of the support on the particle stability opens a possibility to alter the particles support interaction toward a more stable system suitable for heterogeneous catalysis application.

CONCLUSION

In order to assess fundamental questions with respect to the applicability of supported clusters produced in the UHV for organic chemistry transformation, three nonoverlapping size-selected cluster ensembles (Pt_1, $Pt_{n>1}$, and $Pt_{n>35}$) were prepared on Si support (wafer and TEM grids). The Si wafer supported clusters were employed as catalysts for the hydrogenation of *p*-chloronitrobenzene as a benchmark reaction. The catalysts displayed size-dependent activity and remarkably high TON values when compared to recently reported examples of single Pt atoms and subnanometer clusters used for the hydrogenation of nitroarenes.[60,63−65] The calculated TON values show that single atoms display the highest catalytic activity among the studied systems.

XPS characterization of the Pt clusters on the Si wafers before and after application in catalysis shows changes in the oxidation states of the cluster catalysts, aggregation, and a loss of metal into solution after the catalysis experiment. It is very likely, indeed, that catalysis takes place in the homogeneous phase by the detached atoms and clusters, as confirmed by "hot filtration" tests. This result calls for a more careful analysis of the nature of the catalytic reaction when single and few atom clusters are used in wet chemical reactions as this kind of tests were, in general, not performed within comparable studies. Characterization of the corresponding Pt clusters supported on TEM grids by means of HAADF-STEM however, revealed stable clusters before and after exposure to the reaction conditions. This apparent discrepancy between XPS and STEM results can be explained by substantial differences in the support composition of the utilized silicate TEM grids and the wafers, resulting in different catalyst−support interactions.

On the basis of the presented results and the comparison to literature, the following fundamental insights could be gained and answer the questions from the Introduction to a large extent.

The Pt silicate model system is indeed suitable for wet-chemistry conditions. Although the presented test system has not been stable with respect to the support−catalyst interaction (not being a heterogeneous system in the classical sense with respect to robustness and recyclability), still high and size-dependent activity was found. Further investigation should be carried out to clarify if the supported clusters, detaching in solution during the reaction, may represent useful vectors to make highly active, unprotected clusters available as homogeneous catalysts.

Having control of the size down to a single atom and being independent of functional groups, that may alter the catalytic reactivity, this approach seems to be a potential silver bullet for further catalysis studies in the subnanometer range and favorable to the above-mentioned methods of cluster synthesis. Moreover, exploiting the tune-ability of cluster stability by changing support is a promising route toward a truly "heterogeneous" system for future wet chemistry applications that will be explored in future studies.

EXPERIMENTAL SECTION

Sample Preparation. The clusters were deposited on the wafer samples (350 μm thickness, thermally oxidized with an oxide of 50 nm thickness) and Si TEM grids (see details below) using a high frequency laser ablation cluster source and a transfer chamber, described in detail elsewhere.[23,36,58] In brief, the beam of a diode pumped Nd:YAG laser (DPSS Spitlite, 100 Hz, 70 mJ at 532 nm; InnoLas, Germany) was focused onto a rotating (1 Hz) metal target disk (99.99% Pt, Goodfellow, USA). Cooling of the resulting plasma was achieved via a delayed helium (He 6.0, Westfalen, Germany) gas pulse and an adiabatic expansion of the helium−platinum vapor through a nozzle into the vacuum. Ion lenses and an octupole subsequently guided the cluster beam along the axis of a differentially pumped vacuum chamber to a quadrupole bender unit, in which the positively charged clusters were separated from the neutral and negatively charged ones. The deflector was operated in such a way that the cationic clusters were focused into a QMS (ABB Extrel Merlin, U.S.A.) with a mass limit of 16 000 amu where mass selection down to a single cluster size was achieved. The QMS was operated and optimized for highest transmission while still ensuring size selection down to a single mass (see representative mass scans and details on the size distribution in the Supporting Information). For the atom, the QMS ensured deposition of Pt atoms (@ 195 amu) only. Using only the radio frequency (RF only mode) of the QMS, it was operated as a high-pass mass filter. Unselected clusters with a tunable minimum size were generated: starting from either two atoms (cutoff @295 amu) of $Pt_{n>1}$ (excluding the atom) or 36 atoms (cutoff @6980 amu) of $Pt_{n>35}$. After size selection, the beam passed through an aperture of 9 mm and was focused onto the supports (wafer or TEM window). The clusters were deposited under soft-landing conditions on the support, i.e., at deposition energies lower than 1 eV per cluster atom. With recording of the discharge current on the support (coverage reported in unit charges per area: e/nm^2) over the course of the deposition, the coverage of the deposited clusters was determined.

STEM Characterization. Materials and exposure to reaction conditions: The used TEM grids were etched Si wafer grids (TED Pella, U.S.A.) with a silicate support of 8 nm thickness. In order to protect the delicate grid structure from possible mechanical stress during the exposure to reaction conditions, the TEM grids were fixed in a Teflon holder of in-house design in which the window of the grid was exposed to the liquid phase. The holder thereby allowed for the exact same conditions as the wafer, i.e., stirring, reaction vessel, reactants, temperature, etc. After the reaction, the grids were removed

DOI: 10.1021/acscatal.7b00520
ACS Catal. 2017, 7, 4152−4162

from the holder, gently rinsed with the solvent three times, and dried in a nitrogen flow.

STEM measurements were performed at the KAUST analytical core lab, using a FEI Titan 80−300 STEM, equipped with a spherical aberration corrector. The spherical aberration allowed for performing Cs-corrected HR-STEM analysis of samples. We performed the analysis by using a 300 keV energy electron beam, which was focused to a 0.25 nm diameter. Prior to the actual data acquisition, the corrector was aligned to reduce the C3 coefficient of a Condenser-2 (C2) lens to about 1 μm. The HR-STEM images were recorded with a high-angle annular dark field (HAADF) detector by using a typical camera length of 115 mm so that Z-contrast in the images could be enhanced even more than usual in HAADF-STEM imaging.

The analysis of the STEM micrographs was performed using an algorithm of in-house design based on the IGOR Pro 6.22 Particle Analysis Tool (Wavemetrics, USA), previously reported.[38−40,58] The shown statistics for the cluster area (projection), i.e., area distribution functions (ADF) of the $Pt_{n>35}$ clusters are the results of the analysis of multiple images (at least four) and are based on the analysis of at least 400 particles per sample (before: 511 particles and after: 411 particles). Representative STEM micrographs of larger areas for all samples before and after the reaction are shown in the Supporting Information.

XPS Measurements. XPS studies were carried out by means of a Kratos Axis Ultra DLD spectrometer equipped with a monochromatic Al Kα X-ray source ($h\nu$ = 1486.6 eV) operating at 150 W, with a multichannel plate and delay line detector under a vacuum of 1∼10−9 mbar. The survey and high-resolution spectra were collected at fixed analyzer pass energies of 160 and 20 eV, respectively. Binding energies were referenced to the C 1s binding energy of adventitious carbon contamination, which was taken to be 284.8 eV. The data were analyzed with commercially available software, CASAXPS. The metallic peaks were fitted with an asymmetric hybrid Doniach−Sunjic function convoluted with a Gaussian/Lorentzian product, while nonmetallic peaks were fitted with a mixture of Gaussian (70%)−Lorentzian (30%) (GL30) function after Shirley type background subtraction.

Catalytic Experiments. The catalyst was added to a solution of *p*-chloronitrobenzene (157.5 mg, 1.00 mmol, 1 equiv) in 5 mL of ethanol (HPLC grade) in an autoclave. After flushing with hydrogen, a pressure of 5 bar was applied, and the reaction mixture was stirred for 24 h at a temperature of 100 °C. The resulting solution was concentrated to dryness by rotatory evaporation to give a mixture of starting material and *p*-chloroaniline as a white-yellowish solid.

NMR was used as an additional identification method. The spectra were recorded using a standard 400 MHz Bruker spectrometer at room temperature in $CDCl_3$. The chemical shifts are given in δ values (ppm) and refer to the remaining proton signals of the used solvent $CDCl_3$ (δ = 7.26 ppm). For the assignment of the signals and their multiplicities, the following abbreviations were used: d, doublet; br s, broad singlet.

The HPLC-MS method was used for the determination of the *p*-chloroaniline molecular weight and its quantification. The materials are injected into an XDB-phenyl column (ECLIPSE XDB- PHENYL 5u 4.6 × 250 mm Column) then detected by a Vantage Mass Spectrometer (Thermo Scientific) equipped with an electrospray ionization source (APCI) in positive mode. Acetonitrile (LC-MS grade), Milli-Q-Water, and formic acid (MS grade) were used as solvents. Samples were prepared by dissolving 1 mg of solid in 1 mL of acetonitrile. The liquid chromatography (LC) separation was performed using a water/acetonitrile gradient at a flow rate of 0.8 mL/min. The length of the analysis runs was 15 min. The mass spectrometer was set to MRM (multiple reaction monitoring), and the transition was 128 to 93 m/z. The mass spectrometer was equipped with an ESI+ source and run at a heater temperature of 400 °C with sheath gas, 30; auxiliary gas, 15; and a capillary temperature of 275 °C.

Prior to the measurements, a calibration curve in the range from 0 to 10 000 ppb for *p*-chloroaniline with 10 calibration points was recorded to allow for the conversion of peak area to product concentration. The samples were measured each three times and averaged, and the peak area was converted into the product amount using calibration. The obtained values were corrected for the dilution during sample preparation for LC-MS, yielding the absolute total amount of product per measured sample. A summary of the averaged values for each sample type is stated in the Supporting Information (see Table S4), along with the corresponding error. The total error is based on the standard deviation from values of the different samples of the same type, omitting the substantially smaller errors of the LC-MS measurements (the results of the single LC-MS measurements are nearly constant for every sample with a relative error of below 0.5%). Errors for calculated quantities were derived by propagation of uncertainty.

The absolute amount of product molecules was normalized to the amount of cluster on each sample (a value that is measured for each sample as the integrated discharge current during cluster deposition, assuming singly charged clusters).

The conversion from activity per cluster to the activity per individual atom in the cluster was done by dividing through the average number of atoms in a cluster (extracted from the mass scans) as stated in the Supporting Information (see Table S1). The turnover frequency (TOF) per hour stated is derived from the total number of molecules per cluster after the reaction time of 24 h.

■ ASSOCIATED CONTENT

Supporting Information

The Supporting Information is available free of charge on the ACS Publications website at DOI: 10.1021/acscatal.7b00520.

Further details on samples (i.e., size distributions and ranges, mass scans), sample characterization (STEM micrographs, XP survey spectra), and crude NMR spectra of the reaction products as well as substrate conversion values from the LC-MS measurements (PDF)

■ AUTHOR INFORMATION

Corresponding Authors

*E-mail: valerio.delia@vistec.ac.th.

*E-mail: florian.schweinberger@tum.de.

ORCID

Valerio D'Elia: 0000-0002-5881-2496

Jean-Marie Basset: 0000-0003-3166-8882

Present Addresses

⊥Universität Basel, University of Basel - Department of Chemistry, Tiefenbacher Group, St. Johannsring 19, CH-4056 Basel, Switzerland

DOI: 10.1021/acscatal.7b00520
ACS Catal. 2017, 7, 4152−4162

[#]Fritz-Haber-Institute of the Max-Planck-Society − Department of Physical Chemistry, Interfacial Molecular Spectroscopy Group, Faradayweg 4-6, 14195 Berlin, Germany

Author Contributions

The manuscript was written through contributions of all authors. All authors have given approval to the final version of the manuscript.

Notes

The authors declare no competing financial interest.

■ ACKNOWLEDGMENTS

This project was supported through collaboration with the King Abdullah University of Saudi-Arabia (Grant No. KSA-C0069/UKC0020). Further, U.H. and F.F.S. acknowledge financial support through DFG project HE3454/23-1. The authors thank Salim Sioud at the "ACL laboratory" of King Abdullah University of Science and Technology (KAUST) for assistance with the LC-MS measurements and Dr. D. H. Anjum from the "Advanced Nanofabrication Imaging and Characterization" lab at KAUST for his help in acquiring the STEM micrographs. Further, we would like to thank Prof. M. Schuster and co-workers at TUM for their fruitful discussions and clarifications in the field of trace analysis as well as Dr. A. S. Crampton and Dr. C. J. Ridge for their support in the beginning of this study.

■ REFERENCES

(1) Ertl, G. In *Reactions at Solid Surfaces*; John Wiley & Sons: Hoboken, NJ, 2009; pp 123−138.
(2) Bartholomew, C. H.; Farrauto, R. J. Hydrogen Production and Synthesis Gas Reactions. In *Fundamentals of Industrial Catalytic Processes*; John Wiley & Sons: Hoboken, NJ, 2011.
(3) Chorkendorff, I.; Niemantsverdriet, J. W. In *Concepts of Modern Catalysis and Kinetics*; Wiley-VCH Verlag GmbH & Co. KGaA: Weinheim, 2003.
(4) *Bridging Heterogeneous and Homogeneous Catalysis: Concepts, Strategies, and Applications*; Can, L., Yan, L., Eds.; Wiley-VCH Verlag GmbH & Co. KGaA: Weinheim, 2014.
(5) Ertl, G. *Chem. Rec.* **2001**, *1*, 33−45.
(6) Ertl, G. *Pure Appl. Chem.* **1980**, *52*, 2051−2060.
(7) Somorjai, G. A.; Li, Y. In *Introduction to Surface Chemistry and Catalysis*; John Wiley & Sons: Hobokeen, NJ, 2010.
(8) Ertl, G.; Freund, H.-J. *Phys. Today* **1999**, *52*, 32−38.
(9) Thomas, J. M.; Raja, R.; Lewis, D. W. *Angew. Chem., Int. Ed.* **2005**, *44*, 6456−6482.
(10) Copéret, C.; Chabanas, M.; Petroff Saint-Arroman, R.; Basset, J.-M. *Angew. Chem., Int. Ed.* **2003**, *42*, 156−181.
(11) Basset, J.-M.; Baudouin, A.; Bayard, F.; Candy, J.-P.; Copéret, C.; De Mallmann, A.; Godard, G.; Kuntz, E.; Lefebvre, F.; Lucas, C.; Norsic, S.; Pelzer, K.; Quadrelli, A.; Santini, C.; Soulivong, D.; Stoffelbach, F.; Taoufik, M.; Thieuleux, C.; Thivolle-Cazat, J.; Veyre, L. Catalytic Properties of Single Site Catalysts Prepared via Surface Organometallic Chemistry on Oxides and on Metals. In *Modern Surface Organometallic Chemistry*; Basset, J.-M., Psaro, R., Roberto, D., Ugo, R., Eds.; Wiley-VCH Verlag GmbH & Co. KGaA, Weinheim, Germany, 2009.
(12) Copéret, C.; Comas-Vives, A.; Conley, M. P.; Estes, D. P.; Fedorov, A.; Mougel, V.; Nagae, H.; Núñez-Zarur, F.; Zhizhko, P. A. *Chem. Rev.* **2016**, *116*, 323−421.
(13) Pelletier, J. D. A.; Basset, J.-M. *Acc. Chem. Res.* **2016**, *49*, 664−677.
(14) Mazoyer, E.; Merle, N.; Mallmann, A. de; Basset, J.-M.; Berrier, E.; Delevoye, L.; Paul, J.-F.; Nicholas, C. P.; Gauvin, R. M.; Taoufik, M. *Chem. Commun.* **2010**, *46*, 8944−8946.
(15) Basset, J.-M.; Coperet, C.; Soulivong, D.; Taoufik, M.; Cazat, J. T. *Acc. Chem. Res.* **2010**, *43*, 323−334.
(16) Maity, N.; Barman, S.; Callens, E.; Samantaray, M. K.; Abou-Hamad, E.; Minenkov, Y.; D'Elia, V.; Hoffman, A. S.; Widdifield, C. M.; Cavallo, L.; Gates, B. C.; Basset, J.-M. *Chem. Sci.* **2016**, *7*, 1558−1568.
(17) Barman, S.; Maity, N.; Bhatte, K.; Ould-Chikh, S.; Dachwald, O.; Haeßner, C.; Saih, Y.; Abou-Hamad, E.; Llorens, I.; Hazemann, J.-L.; Köhler, K.; D' Elia, V.; Basset, J.-M. *ACS Catal.* **2016**, *6*, 5908−5921.
(18) D'Elia, V.; Dong, H.; Rossini, A. J.; Widdifield, C. M.; Vummaleti, S. V. C.; Minenkov, Y.; Poater, A.; Abou-Hamad, E.; Pelletier, J. D. A.; Cavallo, L.; Emsley, L.; Basset, J.-M. *J. Am. Chem. Soc.* **2015**, *137*, 7728−7739.
(19) Gates, B. C. *Nat. Nanotechnol.* **2008**, *3*, 583−584.
(20) Serna, P.; Gates, B. C. *Acc. Chem. Res.* **2014**, *47*, 2612−2620.
(21) Somorjai, G. A.; York, R. L.; Butcher, D.; Park, J. Y. *Phys. Chem. Chem. Phys.* **2007**, *9*, 3500−3513.
(22) Somorjai, G. A.; Beaumont, S. K.; Alayoglu, S. *Angew. Chem., Int. Ed.* **2011**, *50*, 10116−10129.
(23) Heiz, U.; Vanolli, F.; Trento, L.; Schneider, W.-D. *Rev. Sci. Instrum.* **1997**, *68*, 1986−1994.
(24) Fayet, P.; Patthey, F.; Roy, H.-V.; Detzel, T.; Schneider, W.-D. *Surf. Sci.* **1992**, *269*, 1101−1108.
(25) Kaden, W. E.; Wu, T.; Kunkel, W. A.; Anderson, S. L. *Science* **2009**, *326*, 826−829.
(26) Watanabe, Y.; Isomura, N. *J. Vac. Sci. Technol., A* **2009**, *27*, 1153−1158.
(27) Heiz, U.; Sanchez, A.; Abbet, S.; Schneider, W.-D. *J. Am. Chem. Soc.* **1999**, *121*, 3214−3217.
(28) Sanchez, A.; Abbet, S.; Heiz, U.; Schneider, W.-D.; Häkkinen, H.; Barnett, R. N.; Landman, U. *J. Phys. Chem. A* **1999**, *103*, 9573−9578.
(29) Abbet, S.; Sanchez, A.; Heiz, U.; Schneider, W.-D.; Ferrari, A. M.; Pacchioni, G.; Rösch, N. *J. Am. Chem. Soc.* **2000**, *122*, 3453−3457.
(30) *Model Systems in Catalysis: Single Crystals to Supported Enzyme Mimics*; Rioux, R., Ed.; Springer Science & Business Media: New York, 2009.
(31) Tong, X.; Benz, L.; Kemper, P.; Metiu, H.; Bowers, M. T.; Buratto, S. K. *J. Am. Chem. Soc.* **2005**, *127*, 13516−13518.
(32) Li, F.; Gates, B. C. *J. Phys. Chem. C* **2007**, *111*, 262−267.
(33) Watanabe, Y.; Wu, X.; Hirata, H.; Isomura, N. *Catal. Sci. Technol.* **2011**, *1*, 1490−1495.
(34) Ullman, A. M.; Liu, Y.; Huynh, M.; Bediako, D. K.; Wang, H.; Anderson, B. L.; Powers, D. C.; Breen, J. J.; Abruña, H. D.; Nocera, D. G. *J. Am. Chem. Soc.* **2014**, *136*, 17681−17688.
(35) Vajda, S.; Pellin, M. J.; Greeley, J. P.; Marshall, C. L.; Curtiss, L. A.; Ballentine, G. A.; Elam, J. W.; Catillon-Mucherie, S.; Redfern, P. C.; Mehmood, F.; Zapol, P. *Nat. Mater.* **2009**, *8*, 213−216.
(36) Kunz, S.; Hartl, K.; Nesselberger, M.; Schweinberger, F. F.; Kwon, G.; Hanzlik, M.; Mayrhofer, K. J. J.; Heiz, U.; Arenz, M. *Phys. Chem. Chem. Phys.* **2010**, *12*, 10288−10291.
(37) Nesselberger, M.; Roefzaad, M.; Fayçal Hamou, R.; Ulrich Biedermann, P.; Schweinberger, F. F.; Kunz, S.; Schloegl, K.; Wiberg, G. K. H.; Ashton, S.; Heiz, U.; Mayrhofer, K. J. J.; Arenz, M. *Nat. Mater.* **2013**, *12*, 919−924.
(38) Berr, M. J.; Schweinberger, F. F.; Döblinger, M.; Sanwald, K. E.; Wolff, C.; Breimeier, J.; Crampton, A. S.; Ridge, C. J.; Tschurl, M.; Heiz, U.; Jäckel, F.; Feldmann, J. *Nano Lett.* **2012**, *12*, 5903−5906.
(39) Schweinberger, F. F.; Berr, M. J.; Döblinger, M.; Wolff, C.; Sanwald, K. E.; Crampton, A. S.; Ridge, C. J.; Jäckel, F.; Feldmann, J.; Tschurl, M.; Heiz, U. *J. Am. Chem. Soc.* **2013**, *135*, 13262−13265.
(40) Wettergren, K.; Schweinberger, F. F.; Deiana, D.; Ridge, C. J.; Crampton, A. S.; Rötzer, M. D.; Hansen, T. W.; Zhdanov, V. P.; Heiz, U.; Langhammer, C. *Nano Lett.* **2014**, *14*, 5803−5809.
(41) Riedel, J. N.; Rötzer, M. D.; Jørgensen, M.; Vej-Hansen, U. G.; Pedersen, T.; Sebok, B.; Schweinberger, F. F.; Vesborg, P. C. K.; Hansen, O.; Schiøtz, J.; Heiz, U.; Chorkendorff, I. *Catal. Sci. Technol.* **2016**, *6*, 6893−6900.
(42) Liang, S.; Hao, C.; Shi, Y. *ChemCatChem* **2015**, *7*, 2559−2567.
(43) Thomas, J. M. *Phys. Chem. Chem. Phys.* **2014**, *16*, 7647−7661.

DOI: 10.1021/acscatal.7b00520
ACS Catal. 2017, 7, 4152−4162

(44) Kyriakou, G.; Boucher, M. B.; Jewell, A. D.; Lewis, E. A.; Lawton, T. J.; Baber, A. E.; Tierney, H. L.; Flytzani-Stephanopoulos, M.; Sykes, E. C. H. *Science* **2012**, *335*, 1209−1212.
(45) Yang, M.; Liu, J.; Lee, S.; Zugic, B.; Huang, J.; Allard, L. F.; Flytzani-Stephanopoulos, M. *J. Am. Chem. Soc.* **2015**, *137*, 3470−3473.
(46) Vilé, G.; Albani, D.; Nachtegaal, M.; Chen, Z.; Dontsova, D.; Antonietti, M.; López, N.; Pérez-Ramírez, J. *Angew. Chem., Int. Ed.* **2015**, *54*, 11265−11269.
(47) Liu, W.; Zhang, L.; Yan, W.; Liu, X.; Yang, X.; Miao, S.; Wang, W.; Wang, A.; Zhang, T. *Chem. Sci.* **2016**, *7*, 5758−5764.
(48) Corma, A.; Salnikov, O. G.; Barskiy, D. A.; Kovtunov, K. V.; Koptyug, I. V. *Chem. - Eur. J.* **2015**, *21*, 7012−7015.
(49) Peterson, E. J.; DeLaRiva, A. T.; Lin, S.; Johnson, R. S.; Guo, H.; Miller, J. T.; Hun Kwak, J.; Peden, C. H. F.; Kiefer, B.; Allard, L. F.; Ribeiro, F. H.; Datye, A. K. *Nat. Commun.* **2014**, *5*, 4885.
(50) Qiao, B.; Wang, A.; Yang, X.; Allard, L. F.; Jiang, Z.; Cui, Y.; Liu, J.; Li, J.; Zhang, T. *Nat. Chem.* **2011**, *3*, 634−641.
(51) Kistler, J. D.; Chotigkrai, N.; Xu, P.; Enderle, B.; Praserthdam, P.; Chen, C.-Y.; Browning, N. D.; Gates, B. C. *Angew. Chem., Int. Ed.* **2014**, *53*, 8904−8907.
(52) Jones, J.; Xiong, H.; DeLaRiva, A. T.; Peterson, E. J.; Pham, H.; Challa, S. R.; Qi, G.; Oh, S.; Wiebenga, M. H.; Pereira Hernández, X. I.; Wang, Y.; Datye, A. K. *Science* **2016**, *353*, 150−154.
(53) Zhai, Y.; Pierre, D.; Si, R.; Deng, W.; Ferrin, P.; Nilekar, A. U.; Peng, G.; Herron, J. A.; Bell, D. C.; Saltsburg, H.; Mavrikakis, M.; Flytzani-Stephanopoulos, M. *Science* **2010**, *329*, 1633−1636.
(54) Lucci, F. R.; Marcinkowski, M. D.; Lawton, T. J.; Sykes, E. C. H. *J. Phys. Chem. C* **2015**, *119*, 24351−24357.
(55) Lucci, F. R.; Liu, J.; Marcinkowski, M. D.; Yang, M.; Allard, L. F.; Flytzani-Stephanopoulos, M.; Sykes, E. C. H. *Nat. Commun.* **2015**, *6*, 8550 (2015)..
(56) Wang, J.; Zhao, X.; Lei, N.; Li, L.; Zhang, L.; Xu, S.; Miao, S.; Pan, X.; Wang, A.; Zhang, T. *ChemSusChem* **2016**, *9*, 784−790.
(57) Herzing, A. A.; Kiely, C. J.; Carley, A. F.; Landon, P.; Hutchings, G. J. *Science* **2008**, *321*, 1331−1335.
(58) Schweinberger, F. F. In *Catalysis with Supported Size-selected Pt Clusters*; Springer International Publishing: Cham, Switzerland, 2014.
(59) Eberhardt, W.; Fayet, P.; Cox, D. M.; Fu, Z.; Kaldor, A.; Sherwood, R.; Sondericker, D. *Phys. Rev. Lett.* **1990**, *64*, 780−783.
(60) Peters, S.; Peredkov, S.; Neeb, M.; Eberhardt, W.; Al-Hada, M. *Surf. Sci.* **2013**, *608*, 129−134.
(61) Wei, H.; Liu, X.; Wang, A.; Zhang, L.; Qiao, B.; Yang, X.; Huang, Y.; Miao, S.; Liu, J.; Zhang, T. *Nat. Commun.* **2014**, *5*, 5634.
(62) Zhang, B.; Asakura, H.; Zhang, J.; Zhang, J.; De, S.; Yan, N. *Angew. Chem., Int. Ed.* **2016**, *55*, 8319−8323.
(63) Dhiman, M.; Polshettiwar, V. *J. Mater. Chem. A* **2016**, *4*, 12416−12424.
(64) Xu, G.; Wei, H.; Ren, Y.; Yin, J.; Wang, A.; Zhang, T. *Green Chem.* **2016**, *18*, 1332−1338.
(65) Shimizu, K.; Miyamoto, Y.; Kawasaki, T.; Tanji, T.; Tai, Y.; Satsuma, A. *J. Phys. Chem. C* **2009**, *113*, 17803−17810.
(66) Shimizu, K.; Miyamoto, Y.; Satsuma, A. *J. Catal.* **2010**, *270*, 86−94.
(67) Conceicao, J.; Laaksonen, R. T.; Wang, L.; Guo, T.; Nordlander, P.; Smalley, R. E. *Phys. Rev. B: Condens. Matter Mater. Phys.* **1995**, *51*, 4668−4671.
(68) Corma, A.; Concepción, P.; Boronat, M.; Sabater, M. J.; Navas, J.; Yacaman, M. J.; Larios, E.; Posadas, A.; López-Quintela, M. A.; Buceta, D.; Mendoza, E.; Guilera, G.; Mayoral, A. *Nat. Chem.* **2013**, *5*, 775−781.
(69) Rossell, M. D.; Caparrós, F. J.; Angurell, I.; Muller, G.; Llorca, J.; Seco, M.; Rossell, O. *Catal. Sci. Technol.* **2016**, *6*, 4081−4085.
(70) Qin, Q.; Ma, J.; Liu, K. *J. Colloid Interface Sci.* **2007**, *315*, 80−86.
(71) Zhang, L.; Jiang, J.; Shi, W.; Xia, S.; Ni, Z.; Xiao, X. *RSC Adv.* **2015**, *5*, 34319−34326.
(72) Gelder, E. A.; Jackson, S. D.; Lok, C. M. *Chem. Commun.* **2005**, 522−524.
(73) Gruber-Woelfler, H.; Radaschitz, P. F.; Feenstra, P. W.; Haas, W.; Khinast, J. G. *J. Catal.* **2012**, *286*, 30−40.
(74) Phan, N. T. S.; Van Der Sluys, M.; Jones, C. W. *Adv. Synth. Catal.* **2006**, *348*, 609−679.
(75) Qureshi, Z. S.; Sarawade, P. B.; Albert, M.; D'Elia, V.; Hedhili, M. N.; Köhler, K.; Basset, J.-M. *ChemCatChem* **2015**, *7*, 635−642.
(76) Qureshi, Z. S.; Sarawade, P. B.; Hussain, I.; Zhu, H.; Al-Johani, H.; Anjum, D. H.; Hedhili, M. N.; Maity, N.; D'Elia, V.; Basset, J.-M. *ChemCatChem* **2016**, *8*, 1671−1678.
(77) Drawdy, J. E.; Hoflund, G. B.; Gardner, S. D.; Yngvadottir, E.; Schryer, D. R. *Surf. Interface Anal.* **1990**, *16*, 369−374.
(78) Beier, M. J.; Andanson, J.-M.; Baiker, A. *ACS Catal.* **2012**, *2*, 2587−2595.
(79) Yuan, X.; Yan, N.; Xiao, C.; Li, C.; Fei, Z.; Cai, Z.; Kou, Y.; Dyson, P. J. *Green Chem.* **2010**, *12*, 228−233.
(80) Lara, P.; Suárez, A.; Collière, V.; Philippot, K.; Chaudret, B. *ChemCatChem* **2014**, *6*, 87−90.
(81) Brust, M.; Walker, M.; Bethell, D.; Schiffrin, D. J.; Whyman, R. *J. Chem. Soc., Chem. Commun.* **1994**, *0*, 801−802.
(82) Wang, Y.; Ren, J.; Deng, K.; Gui, L.; Tang, Y. *Chem. Mater.* **2000**, *12*, 1622−1627.
(83) Mafuné, F.; Kohno, J.; Takeda, Y.; Kondow, T.; Sawabe, H. *J. Phys. Chem. B* **2000**, *104*, 9111−9117.
(84) Mafuné, F.; Kohno, J.; Takeda, Y.; Kondow, T. *J. Phys. Chem. B* **2002**, *106*, 8555−8561.
(85) Bradley, J. S.; Tesche, B.; Busser, W.; Maase, M.; Reetz, M. T. *J. Am. Chem. Soc.* **2000**, *122*, 4631−4636.
(86) Zhu, Y.; Qian, H.; Drake, B. A.; Jin, R. *Angew. Chem., Int. Ed.* **2010**, *49*, 1295−1298.
(87) Ohkoshi, S.; Tokoro, H. *Acc. Chem. Res.* **2012**, *45*, 1749−1758.
(88) Imaoka, T.; Kitazawa, H.; Chun, W.-J.; Omura, S.; Albrecht, K.; Yamamoto, K. *J. Am. Chem. Soc.* **2013**, *135*, 13089−13095.
(89) Imaoka, T.; Kitazawa, H.; Chun, W.-J.; Yamamoto, K. *Angew. Chem., Int. Ed.* **2015**, *54*, 9810−9815.
(90) Dai, Y.; Lim, B.; Yang, Y.; Cobley, C. M.; Li, W.; Cho, E. C.; Grayson, B.; Fanson, P. T.; Campbell, C. T.; Sun, Y.; Xia, Y. *Angew. Chem., Int. Ed.* **2010**, *49*, 8165−8168.
(91) Himpsel, F. J.; McFeely, F. R.; Taleb-Ibrahimi, A.; Yarmoff, J. A.; Hollinger, G. *Phys. Rev. B: Condens. Matter Mater. Phys.* **1988**, *38*, 6084−6096.
(92) Parmigiani, F.; Kay, E.; Bagus, P. S. *J. Electron Spectrosc. Relat. Phenom.* **1990**, *50*, 39−46.
(93) McIntyre, N. S.; Cook, M. G. *Anal. Chem.* **1975**, *47*, 2208−2213.
(94) Wanger, C. D.; Riggs, L. E.; Davis, L. E.; Moulder, J. F.; Muilenberg, G. E. In *Handbook of X-Ray Photoelectron Spectroscopy*; Perkin-Elmer Corp.: Waltham, MA, 1979.
(95) Crampton, A. S.; Rötzer, M. D.; Schweinberger, F. F.; Yoon, B.; Landman, U.; Heiz, U. *Angew. Chem., Int. Ed.* **2016**, *55*, 8953−8957.
(96) Ono, L. K.; Yuan, B.; Heinrich, H.; Cuenya, B. R. *J. Phys. Chem. C* **2010**, *114*, 22119−22133.

DOI: 10.1021/acscatal.7b00520
ACS Catal. 2017, 7, 4152−4162